Megakaryocytes build a cage of extracellular matrix that controls their maturation and anchoring to the vascular niche

Short title: Extracellular matrix cage around megakaryocytes

Claire Masson[1≠], Cyril Scandola[2≠], Jean-Yves Rinckel[1], Fabienne Proamer[1], Emily Janus-Bell[1], Fareeha Batool[1], Nael Osmani[3], Jacky Goetz[3], Léa Mallo[1], Catherine Léon[1], Alicia Bornert[1], Renaud Poincloux[4], Olivier Destaing[5], Maxime Lehmann[1], Anita Eckly[1]

≠ Co-authorship

[1]Université de Strasbourg, INSERM, EFS Grand Est, BPPS UMR_S1255, FMTS, F-67065 Strasbourg, France ; [2]Institut Pasteur, Université Paris Cité, Ultrastructural Bioimaging Unit, 75015 Paris, France ; [3]INSERM UMR_S1109, Tumor Biomechanics, Strasbourg F-67000, France ; [4] Institut de Pharmacologie et de Biologie Structurale, Université de Toulouse, CNRS, UMR5089, 205 route de Narbonne, BP64182 31077 Toulouse, France ; [5] Institute for Advanced Biosciences, Centre de Recherche Université Grenoble Alpes, Inserm U 1209, CNRS UMR 5309, Grenoble, France.

Text word count : 3964

Abtract word count : 205

Number of figures : 7

Number of references : 38

Correspondance to: Anita ECKLY

UMR-S1255 INSERM-Université de Strasbourg

Etablissement Français du Sang-Grand Est

10, rue Spielmann, B.P. N°36

67065 Strasbourg Cedex, France

anita.michel@efs.sante.fr

Tel: (33) 388 21 25 25

Fax: (33) 388 21 25 21

Key Points

1. Megakaryocytes form a three-dimensional (3D) cage, composed of laminin and collagen IV, connected to the basement membrane surrounding them. This microarchitecture serves to stabilise megakaryocytes within their vascular niche.
2. Activation of β1/β3 integrins and MMP proteolysis control the microarchitecture of the 3D ECM cage that regulates megakaryocyte maturation and intravasation at the bone marrowblood interface.

Abstract

Megakaryocytes reside in the bone marrow, where they ensure the continuous production of circulating platelets in order to prevent bleeding. Unlike other blood cells, megakaryocytes do not fully enter the bloodstream, but instead extend cytoplasmic protrusions through the sinusoidal barrier, which fragment into circulating platelets. How the extracellular matrix (ECM) regulates the balance between being both resident in the bone marrow and in the bloodstream is still unknown *in vivo.* Here, we address the spatial organisation and functional role of ECM components in the megakaryocyte vascular niche. We reveal that laminin and collagen IV form three-dimensional (3D) cage of ECM connected to the sinusoidal basement membrane that surrounds the individual megakaryocytes. The 3D cages of ECM are controlled by megakaryocytes since megakaryocyte-specific β1/β3 integrin knockout (*Itgb1*$^{-/-}$/*Itgb3*$^{-/-}$) is characterised by weakened ECM cages. This is associated with an increased megakaryocyte intravasation and the passage of entire megakaryocytes into the circulation. The inhibition of ECM degradation induces the formation of denser cages, and results in dysplastic megakaryocytes with defective formation of the demarcation membrane system (DMS). Therefore, the 3D ECM cage stabilizes megakaryocytes within their vascular niche to orchestrate their maturation and intravasation capabilities, and underscores the crucial role of a specific ECM microarchitecture in megakaryocyte functions.

INTRODUCTION

Megakaryocytes, the precursors of blood platelets, differentiate from haematopoietic stem cells and mature in the complex microenvironment of the bone marrow.
Megakaryocytes are large, highly polyploid cells that contain a complex invaginated network of membranes, known as the demarcation membrane system (DMS), which serves as a membrane reservoir for platelet production. These cells are strategically located at the interface between the bone marrow and the blood circulation, specifically at the parasinusoidal region[1,2]. In the final stages of maturation, megakaryocytes extend into the circulation, releasing proplatelet structures which become circulating platelets required for hemostasis[3,4]. The remaining nucleus surrounded by a thin rim of cytoplasm (called the pyrenocyte) is ultimatively phagocytosed in the stroma [5].

Intravasation, the coordinated passage of megakaryocyte fragments through the sinusoidal barrier, is essential for platelet release into the bloodstream. This requires an original, complex and dynamic adaptation of megakaryocytes to highly different microenvironments, both mechanically and biologically. Indeed, they are juxtaposed to the endothelial lining, in an equilibrium between a constrained 3D environment and a fluid environment, where they are in contact with two types of ECM organization: basement membrane and interstitial ECM. Megakaryocytes are themselves able to synthesize and release ECM proteins, thus, contributing to their own structural microenvironment in vascular niches[6]. The importance of the ECM in megakaryocyte development and function has been extensively studied *in vitro* studies, while their mechanistic link *in vivo* are far from being understood. Collagen IV, fibronectin, fibrinogen and laminin α5 chain have already been described around the megakaryocytes *in situ*, whereas, the presence of collagen I and VWF is considered controversial[6-8].

Herein, we demonstrate the specificity, molecular basis and importance of the spatial organization of the ECM around megakaryocytes in native mouse bone marrow. Megakaryocytes assembled a specialized 3D ECM cage composed of a reticular network of laminin and collagen IV, directly connected to the basement membrane of the endothelium. We demonstrated that this 3D cage was organized through the activity of megakaryocyte integrins β1 and β3 since the deletion of both integrins resulted in a severe disruption of its spatial organization. This disorganization leads to an increased megakaryocyte intravasation

and the unexpected passage of whole megakaryocytes into the circulation. Conversely, the use of matrix metalloproteinase (MMP) inhibitors *in vivo* revealed the dynamic process of ECM remodelling that occurs in the maintenance of the ECM cage and its importance for megakaryocyte development, as evidenced by DMS alteration. In conclusion, the 3D ECM cage stabilises megakaryocytes within their vascular niche, thereby enabling the active control of megakaryocyte maturation and intravasation at the interface between the bone marrow and the bloodstream.

METHODS

Detailed methods are described in the Suplemental Data, available on the Web site

Bone marrow preparation. Murine bonne marrow was obtained by flushing the femurs of mice with PBS followed by immediate fixation.

Animals. We used wild type (WT) mice (C57BL/6J from C. River, L'Arbesle, France), Itgb1$^{-/}$/Itgb3$^{-/-}$ double knock out mice and Pf4cre mice aged 10 to 15 weeks. The β1$^{fl/fl}$ [9] and β3$^{fl/fl}$ [10] mice were crossed with mice expressing the Cre recombinase under the control of the Pf4 promoter to obtain inactivation in the MK lineage. *Itgb1$^{-/-}$/Itgb3$^{-/-}$* double knock out (KO) mice were crosses of the two single KO lines.

Antibodies. See table 1 in "Data Supplements S1" for details.

2D confocal microscopy on bone marrow cryosections. Bone marrow were fixed in a mix of 2% paraformaldehyde-0.2% glutaraldehyde, frozen in liquid nitrogen and cut as described [11]. For immunofluorescence staining, 250 nm-thick cryosections were labelled with primary antibodies and conjugated-second antibodies of the appropriate species and DAPI, as reported in table 1. They were examined under a confocal microscope (TCS SP8, Leica) using the 63x objective with a numerical zoom of 4 (pixel size: 0.09µm).

3D confocal analysis on bone marrow vibratome sections. For megakaryocyte localization, sections of femurs or lungs fixed in 2% paraformaldehyde and 0.2% glutaraldehyde, with a thickness of 250 µm, were incubated with FABP4 overnight. This was followed by overnight staining with Alexa 568-conjugated anti-GPIbβ antibody and Alexa 488 Donkey anti-Goat for FABP4. The Leica SP8 confocal microscope was used to collect a series of x-y-z images.

To perform 3D ECM analysis, 250 µm-thick vibratome sections were fixed in 4% PFA and embedded in 4% agarose, incubated overnight at 4°C with an array of antibodies that targeted matrix proteins (laminin, type IV collagen, fibronectin and fibrinogen), and were followed by the corresponding secondary antibodies and Hoechst 33342 counterstaining. For quantitative spatial analysis of ECM around megakaryocyte, the observations have been made on z-stacks

as described by *Voisin et al.* [12]. The fluorescence was delineated on maximum z-stack projection of half a megakaryocyte using Image J software.

Image processing to perform quantitative analyses of fluorescence profiles, pore diameter and fibre length are explained in Suppl. Figure 5.

Intravital imaging. *Pf4cre* and *Itgb1*$^{-/-}$*/Itgb3-/-* mice underwent intravital imaging. To visualize megakaryocytes and sinusoids, an AF488-conjugated anti-GPIX antibody derivative and Qtracker™ 655 were intravenously injected, respectively. The skull bone marrow was observed using two-photon microscopy, following the procedure described in reference[13].

Electron microscopy. For Transmission electron microscopy, bone marrow was fixed in 2.5% glutaraldehyde and embedded in Epon as described [14]. Transversal thinsections of the entire bone marrow were cut and examined under a Jeol 2100 plus. The number of megakaryocytes was counted per surface unit (s.u., 12,945 µm^2).

For SEM, native bone marrow megakaryocytes were allowed to adhere to a surface coated with 300 µg/ml fibronectin, 100 µg/ml fibrinogen or 50 µg/ml laminin 511. After gentle agitation to detach non-adherent cells, the remaining adherent cells were fixed in 2.5 % glutaraldehyde, dehydrated, attached to stubs, sputter coated and examined under a Helios NanoLab microscope at 5kV.

Microfluidic experiments The PDMS microfluidic chamber channels were assembled and connected to peristaltic pump, as described[15]. The channels were washed with PBS for 5 min and coated with laminin 511 (50 µg/ml), fibrillar fibronectin (300 µg/ml) or fibrinogen (100 µg/ml) overnight at 4°C, followed by a blocking stage with human serum albumin (1 %) for 30 min at room temperature. To produce fibrillar fibronectin, we use the method of mechanical stretching as described in Maurer et al, [16]. Freshly isolated megakaryocytes were seeded at a concentration of 30 cells /µL per channel and incubated for 15 min-45 min at 37 °C with 5 % CO_2 (Suppl. Figure 4). The channels were then perfused under a flow of 300 µm/s and the megakaryocyte behavior was monitored in real-time, during 1 min. Megakaryocyte capture

yield was measured by quantifying the number of adherent megakaryocytes before and after flow induction (expressed as a percentage).

Megakaryocyte emigration from bone marrow explants. Preparation of bone marrow explants was performed as described in Guinard et al., 2021 [17]. Briefly, bone marrow from *Pf4cre* or *Itgb1*$^{-/-}$/*Itgb3*$^{-/-}$ mice were flushed and ten 0.5 mm-thick sections were placed in an incubation chamber. Megakaryocytes at the periphery of the explants were counted (expressed as the number of total emigrating megakaryocytes at the indicated timepoints).

Effects of MMP inhibition. Mice were treated daily with a protease inhibitor cocktail (Batimastat at 30 mg/kg + Ilomastat at 50 mg/kg) or vehicle (DMSO dose) for 7 consecutive days [18,19]. On the eighth day, the mice were sacrificed, and their bone marrow was collected for analysis of ECM organization and megakaryocyte behavior, as explained in the 3D confocal analysis on vibratome sections.

Gelatin degradation assay. Coverslips were coated with Oregon green gelatin, fixed with 0.5% glutaraldehyde for 20 min at RT. After washing three times with PBS, cells were seeded on coated coverslips and incubated 6 h before fixation and staining.

Statistics. The homogeneity between different mice was analyzed using a Ki^2 test in order to take all the megakaryocyte data into account. All values are reported as the mean ± sem. n= number of megakaryocytes studied.

RESULTS

1. Laminin and collagen IV create a specialized 3D cage for megakaryocytes in contact with the sinusoidal basement membrane

How the ECM is organized around megakaryocytes within the vascular niche still remains to be discovered as its observation involves technical challenges. We first used ultrathin (250 nm) cryosections and observed megakaryocytes and endothelial cells using GPIbβ and FABP4 markers, respectively. Laminin ϒ1 chain delineated the basement membrane underlying the endothelial layer of sinusoids and the outer contour of mature megakaryocytes (Figure 1A). Collagen IV and fibronectin exhibited similar patterns, whereas fibrinogen was more widespread and predominantly associated with the basement membrane, the megakaryocyte surface and intracellular granules. Von Willebrand factor (VWF) signal was restricted to the alpha granules of megakaryocytes. Notably, collagen I and III signals were undetectable around megakaryocytes and sinusoidal vessels, these antibodies having been validated on positive controls (Suppl. Figure 1).

Having established the expression of laminin, collagen IV, fibronectin and fibrinogen in the direct megakaryocyte microenvironment, their spatial organisation was next investigated using 3D imaging of whole-mount bone marrow preparations (Figure 1B). Maximum Z-stack projections around megakaryocytes were analyzed for each immunostained tissue. Remarkably, this revealed that laminin and collagen form a reticular 3D cage that envelops each megakaryocyte, extending radially from the sinusoidal basement membrane in close association with megakaryocytes (Figure 1C).

To evaluate the relationship between this ECM cage and the sinusoidal basement membrane, we expanded our observations to larger fields of view and performed z-stack analysis around megakaryocytes in contact with sinusoid (sMK in Figure 2A) and megakaryocytes in the parenchyma (pMK in Figure 2A). An overview of the ECM organization is presented in Figure 2A. The quantification revealed that almost all sinusoid-associated megakaryocytes have a cage (92.8 ± 3.3%), while only a few megakaryocytes in the parenchyma displayed this feature (11.4 ± 4.8%), indicating that the 3D ECM cage formation requires megakaryocyte interaction with the sinusoidal basement membrane. Importantly, the cage was present at all stages of megakaryocyte maturation, as defined by their size and the presence of DMS (Suppl. Figure 2A), even during megakaryocyte intravasation (Figure 2B).

Remarkably, 3D representations reveal a deformation of the target megakaryocyte surface that correlates with the presence of the laminin network (white arrows Figure 2C). Finally, the spatial organization of the two other ECM components, fibronectin and fibrinogen present around megakaryocyte, were analyzed. Although fibronectin was readily detected around megakaryocytes, no 3D cages were found for fibronectin and fibrinogen (Suppl. Figures 2B and 2C). Taken together, these observations demonstrate that megakaryocytes establish highly specific interactions with a 3D cage made of laminin and collagen IV, in spatially confined microdomains at the sinusoidal basement membrane.

2. Integrin controls the structural properties of the ECM cage

Megakaryocytes express β1 and β3 integrins as main ECM receptors. To determine the interactions between megakaryocytes and the 3D ECM cages, we localized of the β1 and β3 integrins. Antibodies that bind to all β1 integrins were used to detect β1 isoforms on the plasma membrane and DMS (Figure 3A). Similar findings were obtained for total β3 integrins (Suppl. Figure 3A). In contrast, the activated form of β1 integrin was expressed only at sites of interaction with laminin and collagen IV, suggesting that activated β1 integrins mediate megakaryocyte interactions with the ECM cage (Figure 3B).

To test if integrin-mediated signaling plays a role in the structural assembly of the ECM cage, a transgenic mouse model lacking β1 and β3 integrins specifically in the megakaryocyte lineage (Itgb1$^{-/-}$/Itgb3$^{-/-}$) was used. *Itgb1$^{-/-}$/Itgb3$^{-/-}$* mice were generated by crossing the two single knockout lines (β1$^{fl/fl}$ and β3$^{fl/fl}$ mice crossed with mice expressing the Cre recombinase under the control of the Pf4 promoter). As expected, the activated form of β1 integrin was absent in the megakaryocytes of these mice (Suppl. Figure 3B). Notably, laminin deposition on the megakaryocyte surface was significantly reduced by 2.3 fold in *Itgb1$^{-/-}$/Itgb3$^{-/-}$* mice in comparison to *Pf4Cre* mice (7.1 ± 0.8% vs 18.4 ± 0.9% respectively, measured by fluorescence coverage per unit area) (Figure 3C). Likewise, the intensity fluorescent profiles showed that laminin formed a less dense network around megakaryocytes, with significantly increased pore sizes (10.6 ± 1.3 µm vs 6.3 ± 0.6 µm, respectively). In addition, low ECM density around megakaryocytes in *Itgb1$^{-/-}$/Itgb3$^{-/-}$* mice was most probably not caused by an increased degradation of the matrix, as shown by *in vitro* gelatin degradation assays (Suppl. Figure 3C).

The organization and density of laminin network at the basement membrane remained unaffected in these mice, as the integrin deletion is restricted to megakaryocytes (Suppl. Figure 3D). Finally, a decrease in the expression of fibrillar fibronectin around *Itgb1*$^{-/-}$/*Itgb3*$^{-/-}$ megakaryocytes, along with mislocalization of fibrinogen in the extracellular space of the DMS instead of the granules was also noticed (Suppl. Figures 2B and 2C). Therefore, both megakaryocyte integrins actively organize the 3D ECM cage, and the associated fibronectin and fibrinogen proteins in this cage in the vascular niche.

3. Integrins stabilize megakaryocytes in the vascular niche

The description of this 3D ECM cage raises the question of its functional relevance on megakaryocyte functions. We previously described that *Itgb1*$^{-/-}$/*Itgb3*$^{-/-}$ mice had a 50% reduction in platelet count likely due to disorganized DMS in megakaryocytes[20]. Thus, we hypothesized that the organization of the 3D ECM cage could control the functions of megakaryocytes. Firstly, it appeared that the number of megakaryocytes, the ploidy and the maturation stages in *Itgb1*$^{-/-}$/*Itgb3*$^{-/-}$ mice were similar to those in the control *Pf4cre* mice (Figure 4A). We next analyzed megakaryocyte localization in the bone marrow tissue and found a significantly higher proportion of megakaryocyte that were extending intravascular fragments (i.e. intravasation) in mutant mice (27.0 ± 3.3%) compared to that in *Pf4Cre* mice (2.9 ± 0.4%). More strikingly, intact circulating megakaryocytes were significantly present in their bloodstream (8.2 ± 1.3%) which is an extremely rare (0.7 ± 0.6 %) phenomenon in control mice under physiological conditions (Figure 4B).

To investigate this unusual localization of circulating megakaryocytes in the bloodstream, we used intravital 2-photon microscopy imaging to describe the dynamic of the megakaryocyte behavior. Among megakaryocytes stabilized at the parasinusoidal interface, we could observe the cellular distortions of *Itgb1*$^{-/-}$/*Itgb3*$^{-/-}$ megakaryocytes and their exit from the marrow by entering in the bloodstream intact (Figure 4C, movie 1). Large megakaryocyte nuclei were found in the downstream pulmonary capillaries of these mice (Figure 4D). Such a phenomenon could be due to a difference in size of the megakaryocytes or of the endothelial pores. Transmission electron microscopy (TEM) observation revealed that intravascular *Itgb1*$^{-/-}$/*Itgb3*$^{-/-}$ megakaryocytes were similar in size and ultrastructure to those in the parenchyma compartment (Figure 4E). Furthermore, no significant change in the size of the endothelial

pores (*Itgb1*$^{-/-}$/*Itgb3*$^{-/-}$: 4.6 ± 0.3 µm; WT: 4.3 ± 0.4 µm) was observed, indicating the existence of alternative mechanisms.

Therefore, we measured the adhesive potential of freshly isolated bone marrow megakaryocytes. Under static conditions, most *Itgb1-/-/Itgb3*$^{-/-}$ megakaryocytes did not spread and still showed a round shape on immobilized laminin, fibronectin or fibrinogen (Figure 5A). We then used a miniaturised microfluidic-based experimental model in which individual megakaryocyte detachment was tracked when exposed to a flow rate of 300s-1, similar to the flow typically found in sinusoids (Suppl. Figure 4A). Interestingly, for *Pf4cre* megakaryocytes, it appears that laminin generates less adhesion than other substrates, highlighting the importance of the molecular composition of the said 3D ECM cage and its evident impact on the adhesion response of megakaryocytes *in vivo* (Figure 5B). Experiments using *Itgb1*$^{-/-}$/*Itgb3*$^{-/-}$ megakaryocytes demonstrated significantly higher detachment on various ECM coatings (movies 2 and 3). Secondly, we used the bone marrow explant model to study the adhesion properties of the megakaryocytes associated with their 3D ECM cage (Figure 5C). This model enabled us to quantify the physical detachment of megakaryocyte at the periphery of the explants. After three hours, the number of megakaryocytes released from *Itgb1*$^{-/-}$/*Itgb3*$^{-/-}$ bone marrow explants was significantly higher than that from *Pf4-Cre* explants, reaching a plateau at 6h. Clearly, it appears that β1 and β3 integrins are essential to organize the 3D ECM cages and maintain megakaryocytes in the bone marrow, thereby preventing their passage into the bloodstream as whole cells.

4. 3D ECM cage compression via MMPs inhibition affects the maturation of megakaryocytes

Our results suggest that a weakened ECM cage promotes megakaryocyte intravasation through reduced adhesion. We therefore tested whether an increase in cage density also affects megakaryocyte functions. For that purpose, we proposed to decrease the catabolic aspect occurring in the ECM equilibrium between its synthesis and degradation. To this aim, mice were injected with batimastat (30 mg/kg) and ilomastat (20 mg/kg) for 7 days, in order to inhibit the activation of MMPs in the megakaryocyte microenvironment [21]. Remarkably, this treatment resulted in a significantly denser interstitial collagen IV network, as evidenced by

the abundance of collagen fibres in the interstitial space (Figure 6A). Collagen IV fibre length (6.3 ± 0.2 µm vs 9.3 ± 0.3 µm) and the corresponding pore sizes of the ECM network (4.7 ± 0.3 vs 8.4 ± 0.8 µm) were significantly reduced as compared to the control condition.

We determined if this denser 3D ECM cage might affect megakaryopoiesis. Total megakaryocyte numbers, quantified per bone marrow area using whole bone marrow imaging, revealed a significant 2 fold increase in density in MMP inhibitor-treated mice. In addition, we observed an increased proportion of megakaryocytes with severely reduced size (white arrows in Figure 6B). To better estimate the degree of this defect, we employed TEM and found that 53.7 % of the megakaryocytes lacked the appropriate organization of the DMS (Stage II megakaryocytes), reflecting a primary failure in the cytoplasmic maturation (Figure 6C). In accordance with our IF experiments, TEM analyses also demonstrated a significantly higher number of MK in treated mice, suggesting a greater retention of megakaryocytes in an overcrowded ECM microenvironment. To test this possibility, we quantified the number of MKs released from the bone marrow explants, and observed the release of a significantly fewer megakaryocytes out of the bone marrow microenvironment after 6h as compared to that in control mice (Figure 6D). Together, these results indicate that MMPs are important regulators of ECM homeostasis in the bone marrow, thereby, influencing megakaryocyte maturation and their attachment to the vascular niche.

DISCUSSION

Physiological platelet formation occurs in a complex bone marrow environment where megakaryocytes are located close to sinusoids, suggesting that they are stabilized in a perivascular environment. The present study demonstrates, for the very first time, the existence of a specific 3D ECM cage that stabilizes megakaryocyte to the sinusoids in spatially confined microdomains. The cage consists of a reticular fibre network of laminin and collagen IV that extends radially from the basement membrane and envelops the megakaryocytes. Its structural and adhesive properties are tightly regulated by the interplay between megakaryocyte integrin signaling and ECM proteolysis. Thus, the ECM cage represents a novel concept of an active and dynamic 3D microenvironment continuously remodeled and essential for megakaryocyte perivascular positioning, thereby assisting their maturation and controling their passage from the dense bone marrow environment into the bloodstream (Figure 7).

This study establishes the first images of a hitherto undescribed 3D ECM cage that surrounds megakaryocytes. The presence of the cage throughout their developmental stages, provides further evidence that megakaryocyte maturation occurs while residing at the sinusoid[7]. Likewise, Cai et al. (2022) have showed that deletion of laminin alpha4 in mice reduces vascular-associated megakaryocytes, which in turn affects their maturation and transendothelial proplatelet extension[22]. However, megakaryocytes lacking the main collagen receptors, GPVI and α2β1 integrin, are still able to associate with sinusoids, mature normally, and release platelets into the circulation[23]. This is likely due to the redundant functions of other receptors on the megakaryocyte surface that have collagen and laminin binding capacity, including α6β1, α5β1 and αVβ3 integrins and dystroglycan[8]. One can also imagine that the cage restricts megakaryocyte movement, providing an explanation for the limited migration of megakaryocytes within the bone marrow parenchyma compartment[2,24]. The newly identified ECM cage structure ensures megakaryocyte positioning in the vascular niche plausibly through their reciprocal physical interaction. Besides, the implication of environmental signaling factors such as SDF1 or sphingosine-1-phosphate in materializing this phenomenon has also been reported earlier[25,26].

Integrins are known to have important roles in the remodeling of ECM[27]. Recently, a direct involvement of β1 and β3 integrins in fibrillogenesis of fibronectin has been detected around megakaryocytes[20]. Herein, deletion of β1 and β3 integrins in the megakaryocyte lineage reduces the density and cross-linking of the 3D ECM cage. This is associated with a significant increase in megakaryocyte intravasation events. Our *in vitro* evidences strongly suggest that this effect is due to integrin-mediated adhesion. Our findings, combined with those of Cai et al. who demonstrated reduced sinusoid interaction of megakaryocytes in the absence of laminin α4, highlight the direct involvement of the 3D ECM cage in stabilising megakaryocytes within their vascular niche[22]. This is corroborated by our observations that megakaryocytes, at all maturation stages including the ones captured in the process of shedding intravascular fragments, exhibit a 3D ECM cage. The 3D ECM cage not only anchors the megakaryocytes in the bone marrow but also retains the remnant pyrenocytes at bone marrow-blood interface during the release of platelets, thereby, impeding the sliding away of the entire cell into the blood circulation. Indeed, intact megakaryocytes were found in the general circulation in *Itgb1*$^{-/-}$/*Itgb3*$^{-/-}$ mice. Circulating megakaryocytes have been observed in humans during emergency megakaryopoiesis (infectious diseases, inflammatory diseases, after cardiopulmonary bypass) and have been implicated in thrombotic complications[28-31]. Here, our findings demonstrate that megakaryocyte integrins play a crucial role in determining the density and cross-linking of the 3D ECM cage, which effectively protects megakaryocytes from entering the bloodstream as whole cells.

Administration of MMP inhibitors to mice resulted in an overcrowded and compressed ECM interstitial space (i.e. dense collagen IV meshwork), with hindered megakaryocyte growth. This is similar to what is seen in patients diagnosed with myelofibrosis, where uncontrolled accumulation of ECM is often associated with abnormally small megakaryocytes[32]. Thus, the ECM cage is not just a passive scaffold that anchors megakaryocytes at sinusoids, but its dynamic remodeling also actively contributes to megakaryocyte development. This may reflect an adaptive process whereby the adjustment of the ECM cage facilitates growth by providing enough space for the expansion and development of giant megakaryocytes. This hypothesis aligns with previous findings indicating that increasing the density of the ECM creates a stiffer environment, which affects the growth of individual cells[33,34]. Our 3D representations reveal that the laminin network acts as a

constraint that can physically deform the target megakaryocyte surface. Thus, the ECM cage can present itself as a real barrier with an ability to physically curtail the megakaryocyte at the vascular niche. Besides,megakaryocytes are able to sense substrate stiffness[20,35]. Intriguingly, megakaryocytes rely mostly on β3 subunit for stiffness sensing, whereas, both β1 and β3 integrins are required for fibronectin assembly[20]. Both functions have been reported for other cell models, confirming the essential role of β3 integrin in stiffness sensing and the possible share functions of β1 and β3 integrin on fibrillogenesis[36,37]. Further, the group of K. Hoffmeister showed that proper megakaryocyte localization at the sinusoids depends on β1 integrin glycosylation. The absence of galactosylation in β*4galt1-/-* megakaryocytes leads to hyperactivity of β1 integrin, negatively affecting the formation of the DMS-platelet forming process[38]. Taken together, these data provide evidence of a well-coordinated interplay between integrin-mediated signalling and MMP proteolysis, working together to tightly regulate the mechano-adhesive properties of the ECM cage, and thereby control megakaryocyte maturation at the bone marrow-blood interface.

Overall, the current study demonstrates how the complexity of the 3D ECM microenvironment determines the fate of megakaryocytes in their vascular niche. It highlights the importance of the 3D ECM cage as an active physical scaffold that precisely regulates megakaryocyte positioning and maturation. Maintaining the integrity of the 3D ECM cage and modelling the complex physical constraints that occur in the parasinusoidal region will be important topics for future studies on platelet biogenesis under physiological and stress conditions, particularly in inflammation, where there is an increased incidence of thrombus formation caused by an excess of circulating megakaryocytes.

Acknowledgments

We wish to thank Ketty Knez-Hippert (EFS-GEST) for excellent expert technical assistance. This work was supported by ARMESA (Association de Recherche et Développement en Médecine et Santé Publique) and by ANR Grant MegaPod (ANR-22-CE14-0029).

Authorship Contribution

C.M and C.S performed experiments, analyzed data, and contributed to the writing of the revised manuscript; JY.R, F.P, E.J-B, N.O, J.G, L.M, and A.B. performed experiments, analyzed data, and commented on the manuscript; F.B. and C.L. analyzed data and commented on the manuscript; R.P., O.D, and M.L contributed to the writing of the manuscript; and A.E designed and supervised research, analyzed data, and wrote the manuscript

Discosure of conflicts of interest

The authors have no conflicts of interests to declare

REFERENCES

1. Lichtman MA, Chamberlain JK, Simon W, Santillo PA. Parasinusoidal location of megakaryocytes in marrow: a determinant of platelet release. *Am J Hematol*. 1978;4(4):303-312. 2. Stegner D, vanEeuwijk JMM, Angay O, et al. Thrombopoiesis is spatially regulated by the bone marrow vasculature. *Nat Commun*. 2017;8(1):127.
3. Stone AP, Nascimento TF, Barrachina MN. The bone marrow niche from the inside out: how megakaryocytes are shaped by and shape hematopoiesis. *Blood*. 2022;139(4):483-491.
4. Boscher J, Guinard I, Eckly A, Lanza F, Leon C. Blood platelet formation at a glance. *J Cell Sci*. 2020;133(20).
5. Radley JM, Haller CJ. Fate of senescent megakaryocytes in the bone marrow. *Br J Haematol*. 1983;53(2):277-287.
6. Malara A, Currao M, Gruppi C, et al. Megakaryocytes contribute to the bone marrow-matrix environment by expressing fibronectin, type IV collagen, and laminin. *Stem Cells*. 2014;32(4):926937.
7. Semeniak D, Kulawig R, Stegner D, et al. Proplatelet formation is selectively inhibited by collagen type I through Syk-independent GPVI signaling. *J Cell Sci*. 2016;129(18):3473-3484.
8. Susek KH, Korpos E, Huppert J, et al. Bone marrow laminins influence hematopoietic stem and progenitor cell cycling and homing to the bone marrow. *Matrix Biol*. 2018;67:47-62.
9. Potocnik AJ, Brakebusch C, Fassler R. Fetal and adult hematopoietic stem cells require beta1 integrin function for colonizing fetal liver, spleen, and bone marrow. *Immunity*. 2000;12(6):653-663.
10. Morgan EA, Schneider JG, Baroni TE, et al. Dissection of platelet and myeloid cell defects by conditional targeting of the beta3-integrin subunit. *FASEB J*. 2010;24(4):1117-1127.
11. Eckly A, Scandola C, Oprescu A, et al. Megakaryocytes use in vivo podosome-like structures working collectively to penetrate the endothelial barrier of bone marrow sinusoids. *J Thromb Haemost*. 2020;18(11):2987-3001.
12. Voisin MB, Probstl D, Nourshargh S. Venular basement membranes ubiquitously express matrix protein low-expression regions: characterization in multiple tissues and remodeling during inflammation. *Am J Pathol*. 2010;176(1):482-495.
13. Bornert A, Boscher J, Pertuy F, et al. Cytoskeletal-based mechanisms differently regulate in vivo and in vitro proplatelet formation. *Haematologica*. 2021;106(5):1368-1380.
14. Scandola C, Lanza F, Gachet C, Eckly A. In Situ Exploration of Murine Megakaryopoiesis using Transmission Electron Microscopy. *J Vis Exp*. 2021(175).

15. Osmani N, Follain G, Gensbittel V, Garcia-Leon MJ, Harlepp S, Goetz JG. Probing Intravascular Adhesion and Extravasation of Tumor Cells with Microfluidics. *Methods Mol Biol*. 2021;2294:111-132.
16. Maurer E, Schaff M, Receveur N, et al. Fibrillar cellular fibronectin supports efficient platelet aggregation and procoagulant activity. *Thromb Haemost*. 2015;114(6):1175-1188.
17. Guinard I, Lanza F, Gachet C, Leon C, Eckly A. Proplatelet Formation Dynamics of Mouse Fresh Bone Marrow Explants. *J Vis Exp*. 2021(171).
18. Gui P, Ben-Neji M, Belozertseva E, et al. The Protease-Dependent Mesenchymal Migration of Tumor-Associated Macrophages as a Target in Cancer Immunotherapy. *Cancer Immunol Res*. 2018;6(11):1337-1351.
19. Pielecka-Fortuna J, Kalogeraki E, Fortuna MG, Lowel S. Optimal level activity of matrix metalloproteinases is critical for adult visual plasticity in the healthy and stroke-affected brain. *Elife*. 2015;5:e11290.
20. Guinard I, Nguyen T, Brassard-Jollive N, et al. Matrix stiffness controls megakaryocyte adhesion, fibronectin fibrillogenesis, and proplatelet formation through Itgbeta3. *Blood Adv*. 2023;7(15):4003-4018.
21. Winer A, Adams S, Mignatti P. Matrix Metalloproteinase Inhibitors in Cancer Therapy: Turning Past Failures Into Future Successes. *Mol Cancer Ther*. 2018;17(6):1147-1155.
22. Cai H, Kondo M, Sandhow L, et al. Critical role of Lama4 for hematopoiesis regeneration and acute myeloid leukemia progression. *Blood*. 2022;139(20):3040-3057.
23. Semeniak D, Faber K, Oftering P, Manukjan G, Schulze H. Impact of Itga2-Gp6-double collagen receptor deficient mice for bone marrow megakaryocytes and platelets. *PLoS One*. 2019;14(8):e0216839.
24. Junt T, Schulze H, Chen Z, et al. Dynamic visualization of thrombopoiesis within bone marrow. *Science*. 2007;317(5845):1767-1770.
25. Avecilla ST, Hattori K, Heissig B, et al. Chemokine-mediated interaction of hematopoietic progenitors with the bone marrow vascular niche is required for thrombopoiesis. *Nat Med*. 2004;10(1):64-71.
26. Zhang L, Orban M, Lorenz M, et al. A novel role of sphingosine 1-phosphate receptor S1pr1 in mouse thrombopoiesis. *J Exp Med*. 2012;209(12):2165-2181.
27. Berrier AL, Yamada KM. Cell-matrix adhesion. *J Cell Physiol*. 2007;213(3):565-573.
28. Gelon L, Fromont L, Lefrancais E. Occurrence and role of lung megakaryocytes in infection and inflammation. *Front Immunol*. 2022;13:1029223.
29. Puhm F, Laroche A, Boilard E. Diversity of Megakaryocytes. *Arterioscler Thromb Vasc Biol*. 2023;43(11):2088-2098.
30. Rapkiewicz AV, Mai X, Carsons SE, et al. Megakaryocytes and platelet-fibrin thrombi characterize multi-organ thrombosis at autopsy in COVID-19: A case series. *EClinicalMedicine*. 2020;24:100434.
31. Frydman GH, Ellett F, Jorgensen J, et al. Megakaryocytes respond during sepsis and display innate immune cell behaviors. *Front Immunol*. 2023;14:1083339.
32. Gianelli U, Thiele J, Orazi A, et al. International Consensus Classification of myeloid and lymphoid neoplasms: myeloproliferative neoplasms. *Virchows Arch*. 2023;482(1):53-68.
33. Barriga EH, Franze K, Charras G, Mayor R. Tissue stiffening coordinates morphogenesis by triggering collective cell migration in vivo. *Nature*. 2018;554(7693):523-527.
34. Dolega ME, Monnier S, Brunel B, Joanny JF, Recho P, Cappello G. Extracellular matrix in multicellular aggregates acts as a pressure sensor controlling cell proliferation and motility. *Elife*. 2021;10.

35. Aguilar A, Pertuy F, Eckly A, et al. Importance of environmental stiffness for megakaryocyte differentiation and proplatelet formation. *Blood*. 2016;128(16):2022-2032.
36. De Mets R, Wang I, Balland M, et al. Cellular tension encodes local Src-dependent differential beta(1) and beta(3) integrin mobility. *Mol Biol Cell*. 2019;30(2):181-190.
37. Kyumurkov A, Bouin AP, Boissan M, et al. Force tuning through regulation of clathrindependent integrin endocytosis. *J Cell Biol*. 2023;222(1).
38. Giannini S, Lee-Sundlov MM, Rivadeneyra L, et al. beta4GALT1 controls beta1 integrin function to govern thrombopoiesis and hematopoietic stem cell homeostasis. *Nat Commun*. 2020;11(1):356.

Figure Legends

Figure 1

Laminin and collagen IV form a specialized 3D cages of ECM for megakaryocytes, directly connected to the sinusoidal basement membrane

(A) Left panel. Schematic representation of the experimental workflow for 2D imaging of immunostained bone marrow cryosections from WT mice. Confocal imaging is performed on single ultrathin sections with an axial resolution of 250 µm. Right panel. Representative 2D images of a sinusoid-associated MK immunostained for laminin (red), GPIbβ (white) and FABP4 (cyan). Cell nuclei are visualized with DAPI (blue) (from one out of three independent IF experiments).

(B) Left panel. Schematic representation of the experimental workflow for 3D analysis of whole-mount bone marrow preparations from WT mice. A stack of confocal images covering half the depth of the MK is acquired and then z-projected to create a maximum projection image. Right panel. Representative 3D images of sinusoid-associated MK immunostained for laminin (red), GPIbβ (white) and FABP4 (cyan) (from one out of three independent IF experiments).

(C) Left panel. Representative 3D images of sinusoid-associated MK immunostained for collagen IV (green) and GPIbβ (white). Right panel. Laminin (red) and collagen IV (green) colocalize around sinusoid-associated MK.

*, sinusoid lumen; arrowheads, basement membrane-cage connexion; bm, basement membrane ; MK, megakaryocyte; P, platelet; Bars, 10 µm.

Figure 2

The ECM cage interacts mechanically with megakaryocytes at the sinusoid

(A) The spatial distribution of ECM cage is highly restrictive to the sinusoid. Maximal projection of a large field of the 3D laminin organization. Megakaryocytes in contact with sinusoids (sMK) have a cage. Quantification of the number of megakaryocytes displaying the typical 3D cage as a function of cell association with sinusoids. Megakaryocytes with an ECM cage (grey bars) and without a cage (hatched bars) were counted (from 3 independent experiments, $3<n<101$ as indicated in/over the bars, **$P<0.01$ Mann-Whitney).

(B) Correlation with the maturation stages of megakaryocytes. Maximal projections of semimegakaryocytes are shown. Quantification of laminin immunostaining per cell shows the presence of a 3D ECM cave at all stages of maturation (2-3 independent experiments, 14<n<22 as indicated in the bars, *P<0,05 Mann-Whitney). Quantification on megakaryocytes extending proplatelets and pyrenocytes (nacked nucleus) was not possible due to sample size limitations. Note that the characterization of maturation stages is shown in Suppl. Figure 2.

(C) Representative confocal image of a megakaryocyte displaying a laminin cage and its 3D construction showing that the laminin network (red) deforms the megakaryocyte surface (white arrows). Zoom show 3D surface rendering of the physically deformation of megakaryocyte surface.

*, sinusoid lumen; bm, basement membrane; MK, megakaryocyte; sMK, sinusoid-associated MK; pMK, MK in the parenchyma; PPT, proplatelet; n=number of cells studied; Bar, 10 µm**.**

Figure 3

Integrin-mediated control of the 3D ECM cage around MK.

(A) Representative 2D images of *Pf4cre* bone marrowcryosections (250 nm) showing a sinusoid-associated MK immunostained for β1 integrin (MAB1997 in yellow). Right: the boxed area isshown at a higher magnification.

(B) Activated β1 integrins form functional adhesion structures around MK surfaces. Representative 2D images of of *Pf4cre* bone marrow cryosections showing a sinusoidassociated MK immunostained for activated β1 integrin (9EG7 in cyan), for GPIbb (white) and laminin (red, upper panels) or collagen IV (green, lower panels). Right: Magnification of the boxed area showing co-localization of laminin and 9EG7.

(C) Deletion of β1 and β3 integrins leads to a reduction in the laminin deposition on the surface of MKs. Upper panels. Representative 3D images showing a decrease in laminin deposition (red) on *Itgb1*$^{-/-}$*/Itgb3*$^{-/-}$ MK compared to *Pf4cre.* Top panels. (Left) Quantification of laminin surface coverage per MK (in %, 17<n<19 as indicated in the bars, P>0.001 unpaired t-Test), (Middle) expression profile of the laminin staining along straight-lines (25 µm long) visible as white lines in the confocal images, and (Right) quantification of mesh sizes (in µm, 14<n<16, P<0.01 Mann-Whitney).

*, sinusoid lumen; pm, plasma membrane; MFI, mean fluorescence intensity; MK, megakaryocyte; n=number of cells studied; Bars, 10 µm.

Figure 4

Integrins protect megakaryocytes from entering the bloodstream as whole cells

(A) Megakaryocyte density, maturation and ploidy were normal in *Itgb1*$^{-/-}$/*Itgb3*$^{-/-}$ BM. (Left) Quantification of the total number of megakaryocyte, observed by electron microscopy (from 6-7 independent experiments, 120<n<153 as indicated in the bars), (Middle) Classification of the megakaryocytes according to their maturation stage (from 3-5 independent experiments, 99<n<544). (Right) Representative ploidy histograms of *Pf4cre* and *Itgb1*$^{-/-}$/*Itgb3*$^{-/-}$ megakaryocyte (one out of three independent experiments).

(B)Higher proportion of megakaryocytes extending intravascular proplatelets (intravasation) in mice lacking β1/β3 integrins. Representative confocal images of *Pf4cre* and *Itgb1*$^{-/-}$/*Itgb3*$^{-/-}$ whole-mount bone marrow immunostained for GPIbβ (white) and FABP4 (cyan). Zoomed-in images (right) reveal an *Pf4cre* intravasating megakaryocyte and a circulating *Itgb1-/-/Itgb3/-* megakaryocyte. Quantification of megakaryocyte localization (n=5 for each genotype, 200<n<225 as indicated in the legend, *** P<0.001 Mann Whitney).

(C) Intravital two-photon imaging of *Itgb1*$^{-/-}$/*Itgb3*$^{-/-}$ mouse calvarial bone marrowstained with intravenously injected AF488-conjugated anti-GPIX antibody and rhodamin dextran. The white arrow indicates an intrasinusoidal *Itgb1*$^{-/-}$/*Itgb3*$^{-/-}$ megakaryocyte, dotted lines illustrate the sinusoid wall and the values in the left corner show the time-lapses. Quantification of circulating megakaryocytes, data are reported as the percentage of the total number of megakaryocyte (from 3 independent experiments, 130<n<136 as indicated in the legend, P<0.05, Mann-Whitney).

(D) Increased number of megakaryocyte pyrenocytes (nacked nuclei) within the pulmonary microvessels of *Itgb1*$^{-/-}$/*Itgb3*$^{-/-}$ mice. Megakaryocytes are identified by GPIbβ staining (green) and nuclei are visualized by DAPI staining (blue, arrow). Cyan dotted lines indicate the vessel wall. Quantification of the remaining nuclei in *Pf4cre* (grey) and *Itgb1*$^{-/-}$/*Itgb3*$^{-/-}$ (black) mice (from 5 independent experiments, 28<n<149 as indicated in bars, ***P*<0.01, Mann-Whitney (E) (Left) TEM image demonstrating the typical intravasation behaviour of a megakaryocyte, which is characterized by the extension of intravascular

proplatelets, (Middle - Right) Two TEM images showing intravascular entire *Itgb1-/-/Itgb3-/-* MKs.

*, sinusoid lumen; cyan dotted line, sinusoid wall ; n, nucleus; sMK, sinusoid-associated MK; pMK, MK in the parenchyma; PPT, proplatelets; cyan dotted line, sinusoid wall; n= number of cells studied, Bars in B-C-D, 10 µm; Bars in E, 5 µm.

Figure 5

Integrins promote megakaryocyte adhesion to the ECM components of the bone marrow (A) Impaired adhesion and spreading of *Itgb1*$^{-/-}$*/Itgb3*$^{-/-}$ MK. Representative SEM images depicting bone marrow-derived megakaryocytes adhering on laminin. Spreading (hatched bars) and round (grey bars) megakaryocytes were counted following 3h incubation on laminin, fibronectin (FN), and fibrinogen (FG) (in %) (from 4-6 independent experiments, n as indicated in the legends).

(B) Microfluidic flow chamber to study megakaryocyte adhesion efficiency. Representatives bright field images showing that upon flow application, *Itgb1*$^{-/-}$*/Itgb3*$^{-/-}$ megakaryocytes detach from fibrillary fibronectin protein, while *Pf4Cre* MKs remain attached. Quantification of the detachment of *Pf4cre* and *Itgb1*$^{-/-}$*/Itgb3*$^{-/-}$ megakaryocytes on laminin, fibrillar fibronectin and fibrinogen (from 5 to 7 independent experiments , n as indicated in the legends, **P<0.01, ***P<0,001, Mann-Whitney).

(C) Reduced physical anchoring of *Itgb1*$^{-/-}$*/Itgb3*$^{-/-}$ megakaryocytes to bone marrow. Representatives bright field images of the ten femur bone marrowsections placed in an incubation chamber (left panel), of the box (center panel) and of the megakaryocytes released from the periphery of the explants (right panel). Quantification of the number of *Pf4cre* and *Itgb1*$^{-/-}$*/Itgb3*$^{-/-}$ megakaryocytes released from the explants following 3h (from 10 to 13 independent experiments, 594<n<1095 for Pf4cre and *Itgb1*$^{-/-}$*/Itgb3*$^{-/-}$, *P<0.05, unpaired ttest).

dotted lines, MK detachment; MK, megakaryocytes, FN, fibronectin; FG, fibrinogen; MK, megakaryocytes, n, number of cells studied; Bars in A, 10 µm; Bars in B, 20 µm; Bars in B, 30 µm.

Figure 6

Maturation of the 3D ECM cage is correlated with maturation of the DMS in megakaryocytes

(A) MMP inhibition leads to a densification of the peri-MK cage. Upper panels. Representative 3D confocal images showing a significant increase in collagen IV deposition (green) on the megakaryocyte surface in treated mice treated with the intravenous cocktail of protease inhibitors (B + I). Top panels. (Left) Quantification of collagen IV fluorescence showed a shortening of collagen IV fibers in treated mice compared to that in control mice (from 3-5 independent experiments, 20<n<22 as indicated in the bars, ***P<0;001, Mann-Whitney). (Middle) Histograms of fluorescence intensity versus distance showed an increase in crosslinking with a reduction in pore size (white lines of 25µm length are visible in the confocal images). (Right) Reduction in mesh sizes in treated mice (from 3 independent experiments, 7<n<12, ***P>0.001, t-test).

(B) MMP inhibition affects megakaryocyte growth (indicated by arrows). Representativebone marowconfocal images from DMSO *vs* B+I treated mice immunostained for GPIbβ (white) and FABP4 (cyan), zoomed-in images showing the difference in megakaryocyte size between the two groups. Quantification of the number of megakaryocytes per bone marrow area (194 x 194 µm) (from 3 independent experiments, 229<n<483 as indicated in the bars, ***P<0.0001, Mann-Whitney).

(C) TEM observation revealed the presence of numerous immature megakaryocytes (stage II) in treated mice as compared to fully mature megakaryocytes in control mice (stage III). (Middle) Quantification of the total number of megakaryocyte s (145<n<169 as indicated in bars, **P<0.01, Mann-Whitney) and in the proportion of immature megakaryocytes (stage II) in the B + I group (from 3 independent experiments, *P < 0.05, **P < 0.01, one way ANOVA Dunn's).

(D) Representatives bright field images of the megakaryocytes (arrows) released from the periphery of the control and treated explants. Quantification of the number of megakaryocytes released from the explants following 3h and 6h (from 6 independent experiments, 370<n<783 for DMSO and B+I, *P<0.05, unpaired t-test).

B + I, batimastat + Ilomastat; sMK, sinusoid-associated MK; pMK, MK in the parenchyma; n, number of cells studied; Bars in A and B, 10 µm; Bars in C, 5 µm; Bar in D, 50 µm.

Figure 7

β1/β3 Integrins and MMP proteolysis control the 3D ECM cage microarchitecture that regulates megakaryocyte maturation and intravasation at the bone marrow-blood interface.

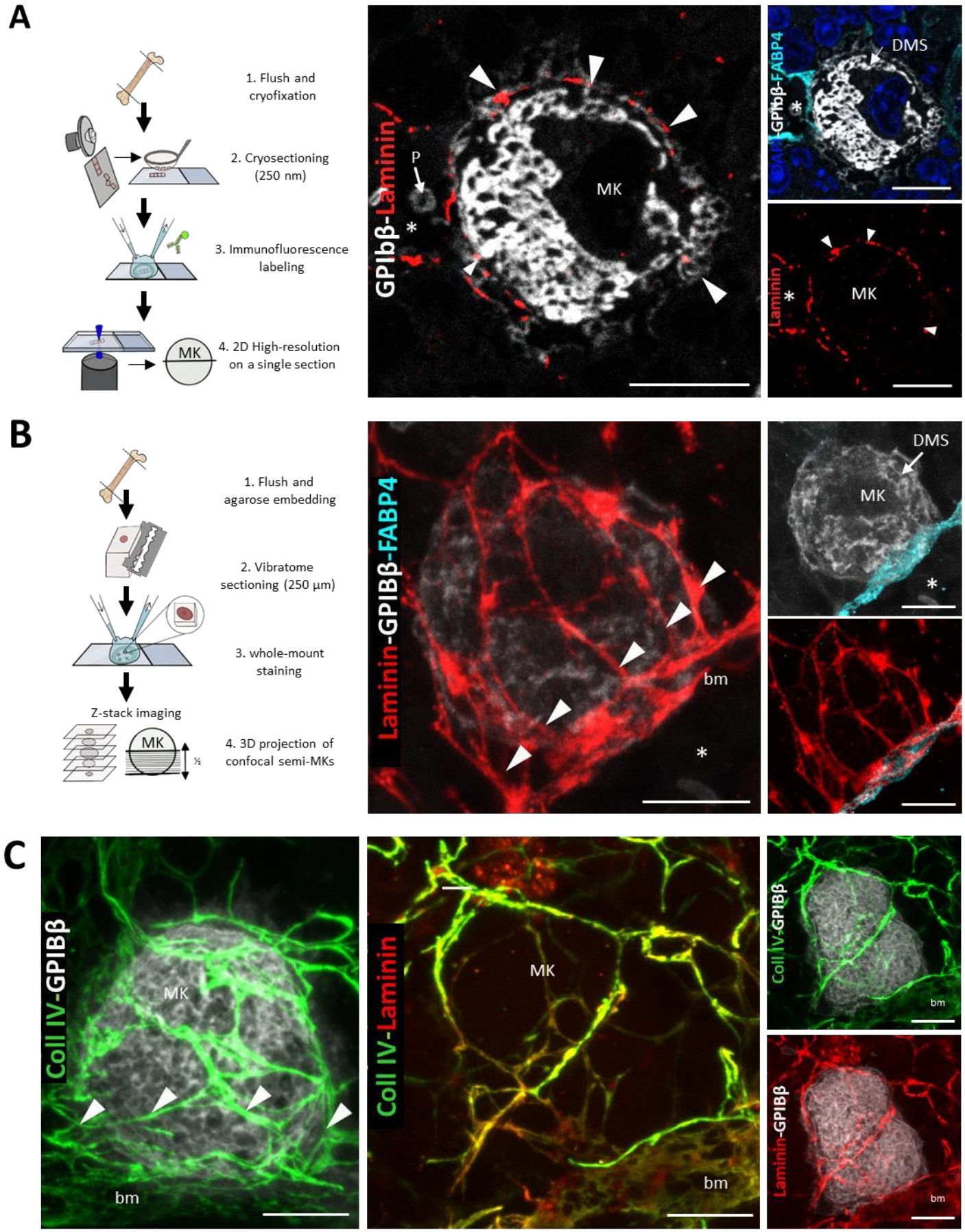
A
1. Flush and cryofixation
2. Cryosectioning (250 nm)
3. Immunofluorescence labeling
MK
4. 2D High-resolution on a single section
GPIbβ-Laminin
P
*
MK
DAPI-GPIbβ-FABP4
DMS
*
Laminin
*
MK
B
1. Flush and agarose embedding
2. Vibratome sectioning (250 µm)
3. whole-mount staining
Z-stack imaging
MK
½
4. 3D projection of confocal semi-MKs
Laminin-GPIBβ-FABP4
bm
*
DMS
MK
*
C
Coll IV-GPIBβ
MK
bm
Coll IV-Laminin
MK
bm
Coll IV-GPIBβ
bm
Laminin-GPIBβ
bm

Figure 1

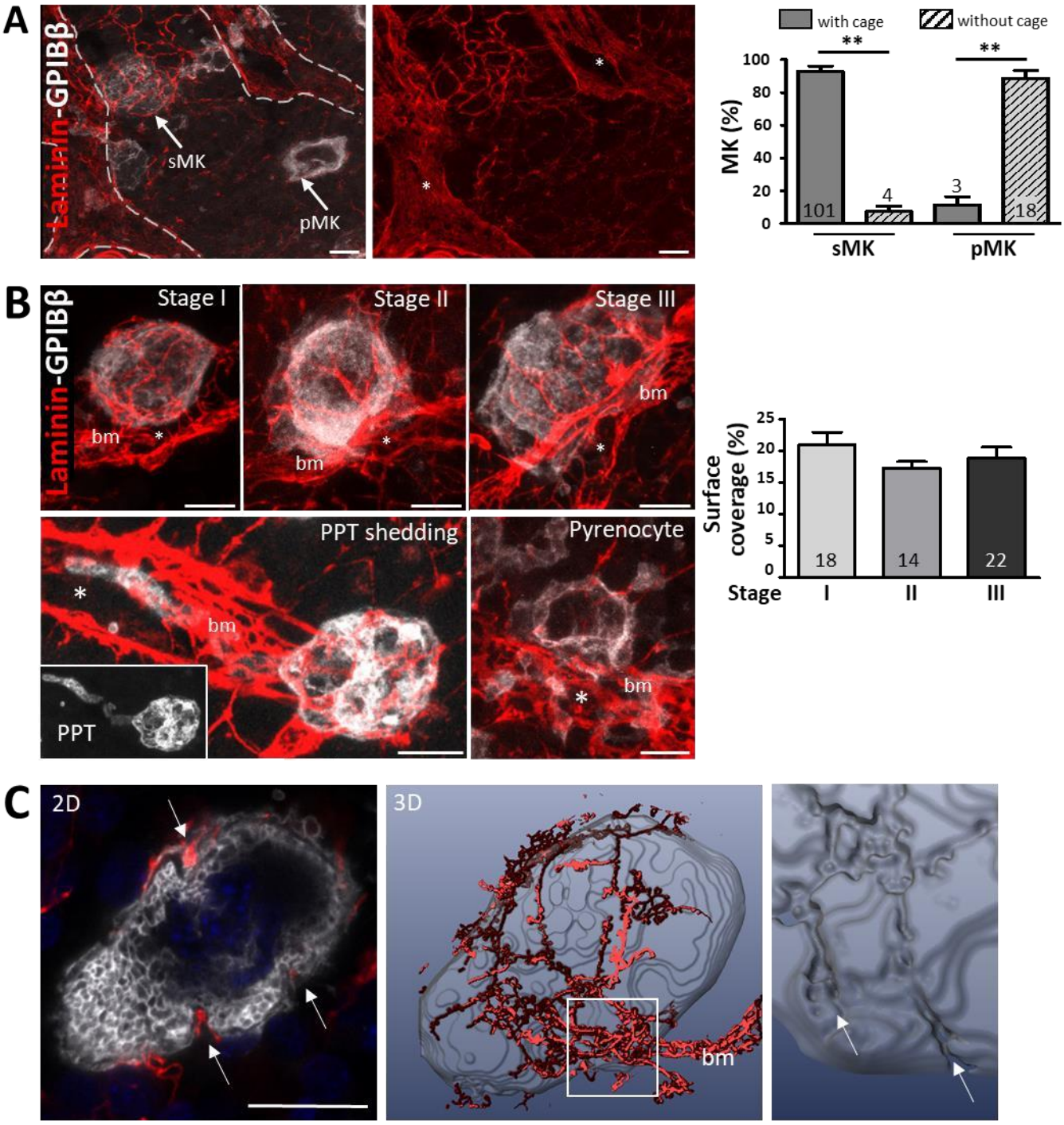
A
Laminin-GPIBβ
sMK
pMK
with cage
without cage
**
**
MK (%)
100
80
60
40
20
0
101
4
3
18
sMK
pMK
B
Laminin-GPIBβ
Stage I
Stage II
Stage III
bm
PPT shedding
Pyrenocyte
PPT
Surface coverage (%)
25
20
15
10
5
0
18
14
22
Stage
I
II
III
C
2D
3D
bm

Figure 2

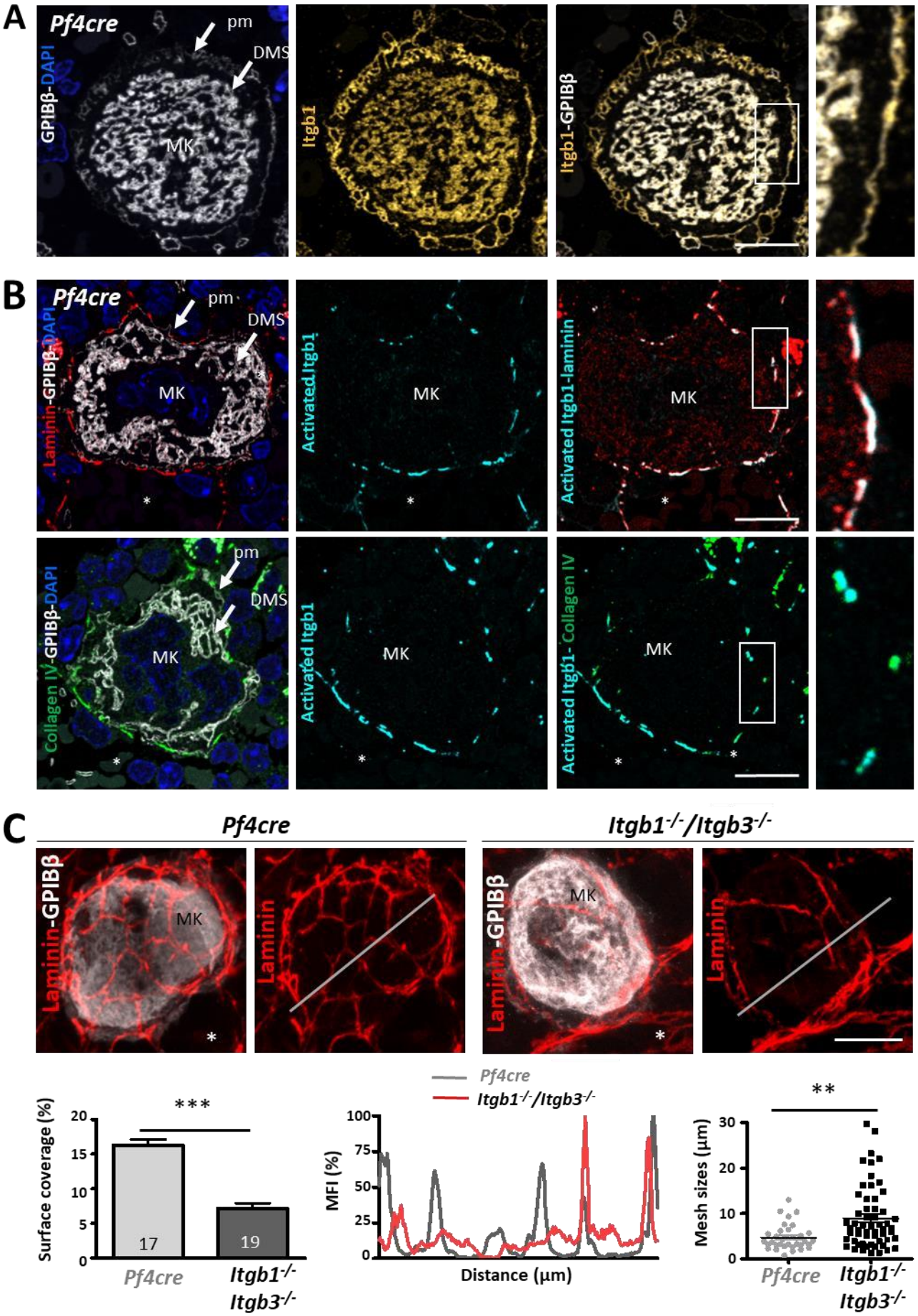
A
Pf4cre
pm
DMS
GPIBβ-DAPI
MK
Itgb1
Itgb1-GPIBβ
B
Pf4cre
pm
DMS
Laminin-GPIBβ-DAPI
MK
ActivatedItgb1
Activated Itgb1-laminin
Collagen IV-GPIBβ-DAPI
Activated Itgb1
Activated Itgb1- Collagen IV
C
Pf4cre
Itgb1-/-/Itgb3-/-
Laminin-GPIBβ
Laminin
Surface coverage (%)
***
17
19
Pf4cre
Itgb1-/-
Itgb3-/-
MFI (%)
Distance (µm)
Mesh sizes (µm)
**

Figure 3

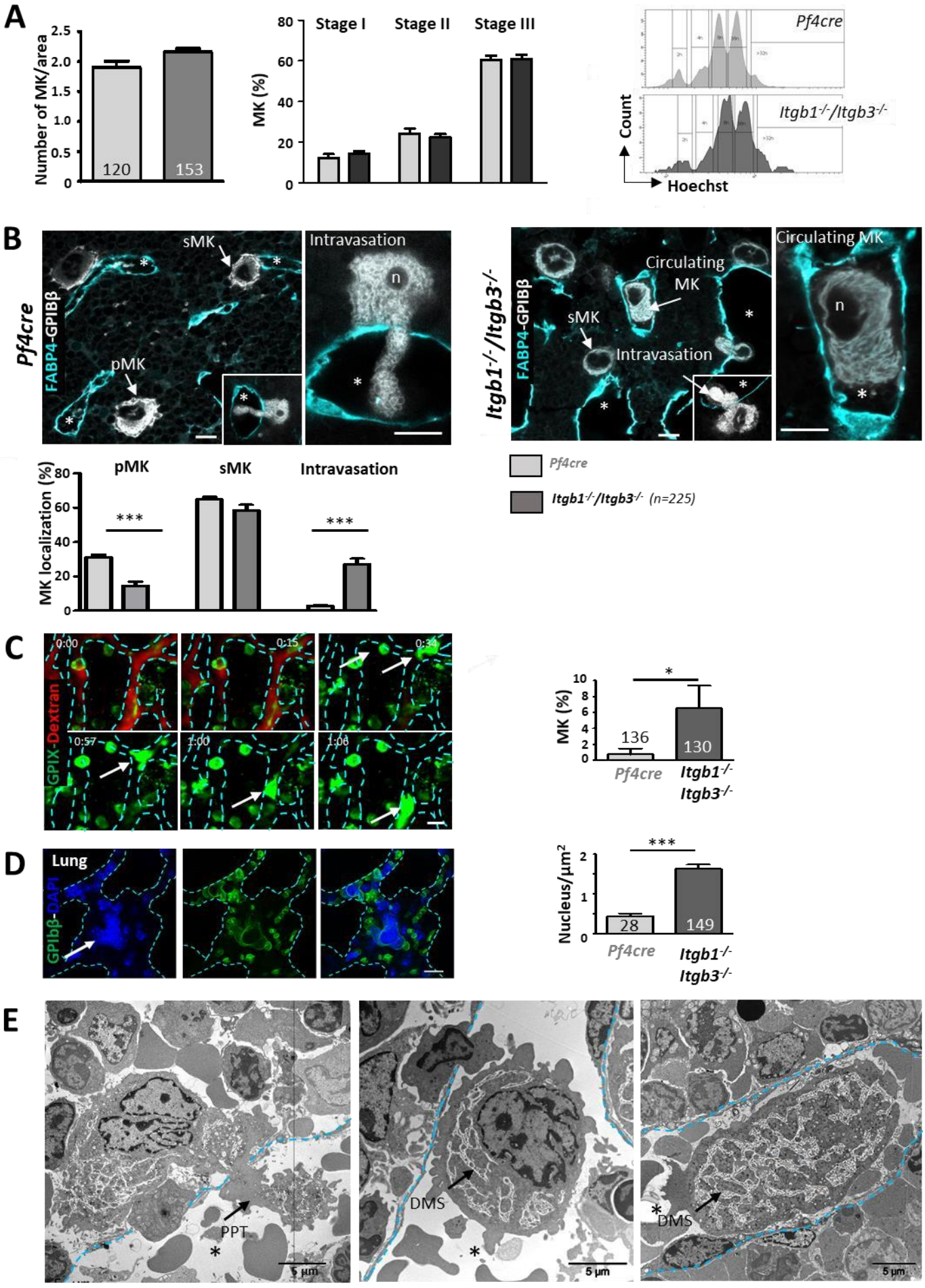
A
Number of MK/area
120
153
Stage I
Stage II
Stage III
MK (%)
Pf4cre
Itgb1-/-/Itgb3-/-
Count
Hoechst
B
Pf4cre
FABP4-GPIBβ
sMK
pMK
Intravasation
n
Itgb1-/-/Itgb3-/-
Circulating MK
MK localization (%)
pMK
sMK
Intravasation
***
Pf4cre
Itgb1-/-/Itgb3-/- (n=225)
C
GPIX-Dextran
0:00
0:15
0:34
0:57
1:00
1:06
MK (%)
136
130
Pf4cre
Itgb1-/-
Itgb3-/-
D
Lung
GPIbβ-DAPI
Nucleus/µm2
28
149
E
PPT
DMS
5 µm

Figure 4

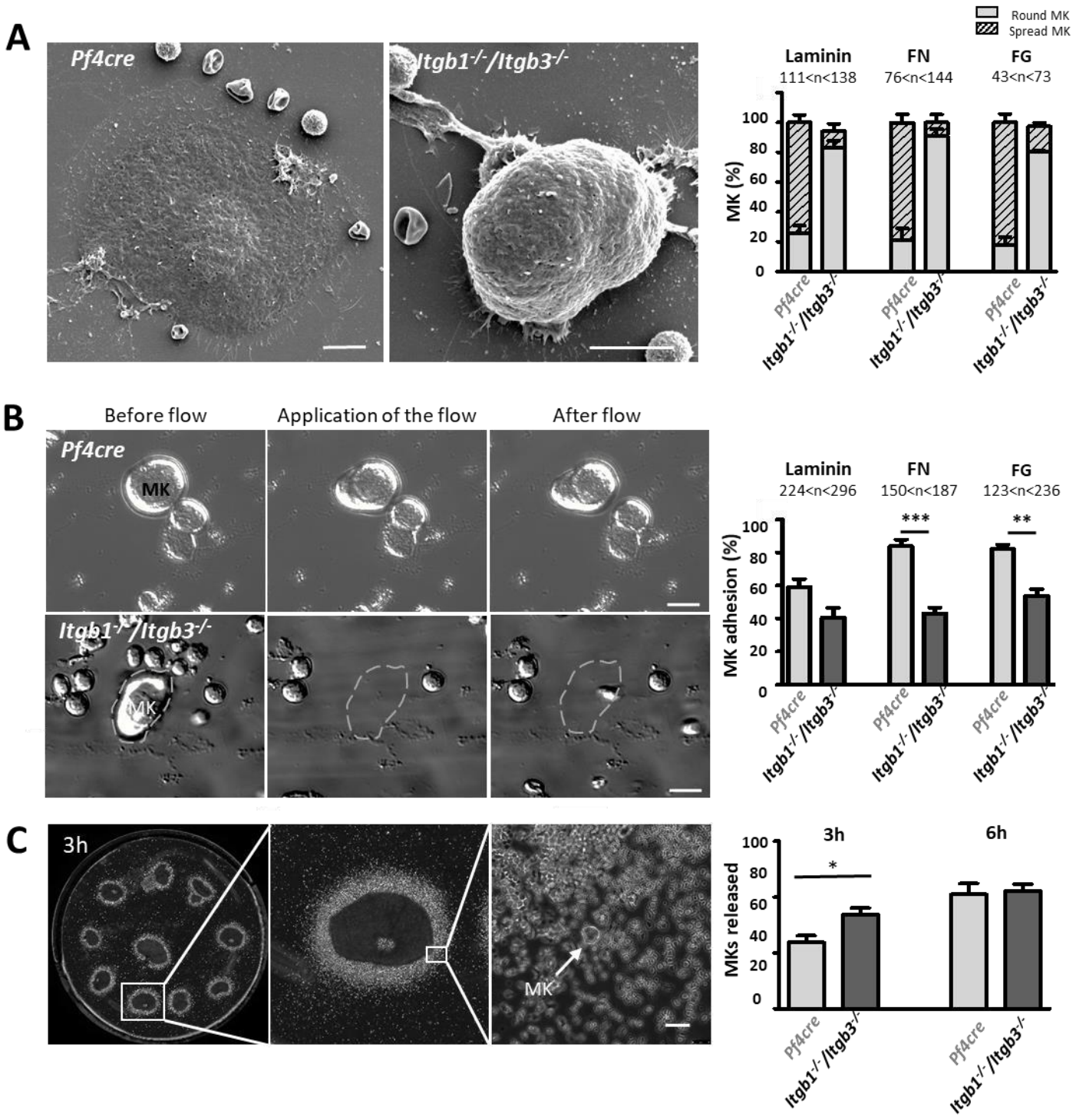
A
Pf4cre
Itgb1-/-/Itgb3-/-
Round MK
Spread MK
Laminin
111<n<138
FN
76<n<144
FG
43<n<73
MK (%)
100
80
60
40
20
0
Pf4cre
Itgb1-/-/Itgb3-/-
B
Before flow
Application of the flow
After flow
MK
Laminin
224<n<296
FN
150<n<187
FG
123<n<236
***
**
MK adhesion (%)
C
3h
MK
3h
6h
*
MKs released

Figure 5

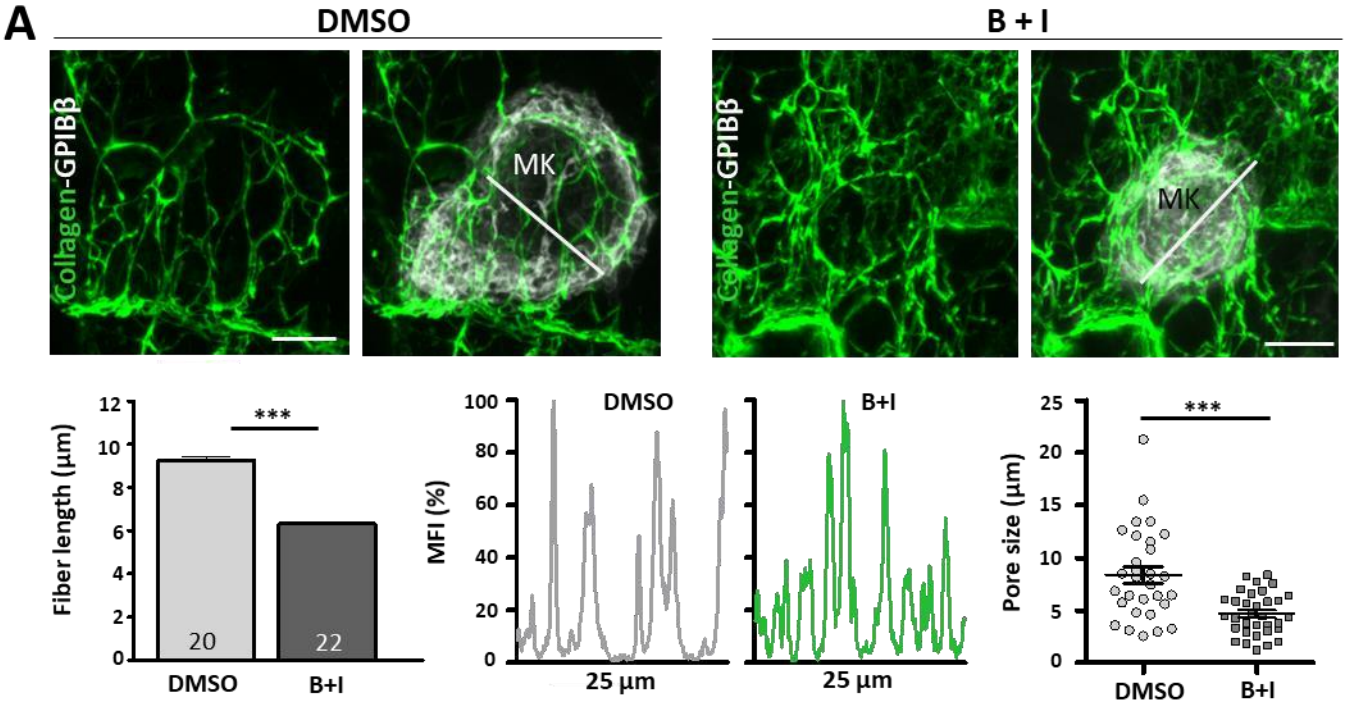
A
DMSO
B + I
Collagen-GPIBβ
MK
Fiber length (µm)
***
20
22
DMSO
B+I
MFI (%)
25 µm
Pore size (µm)

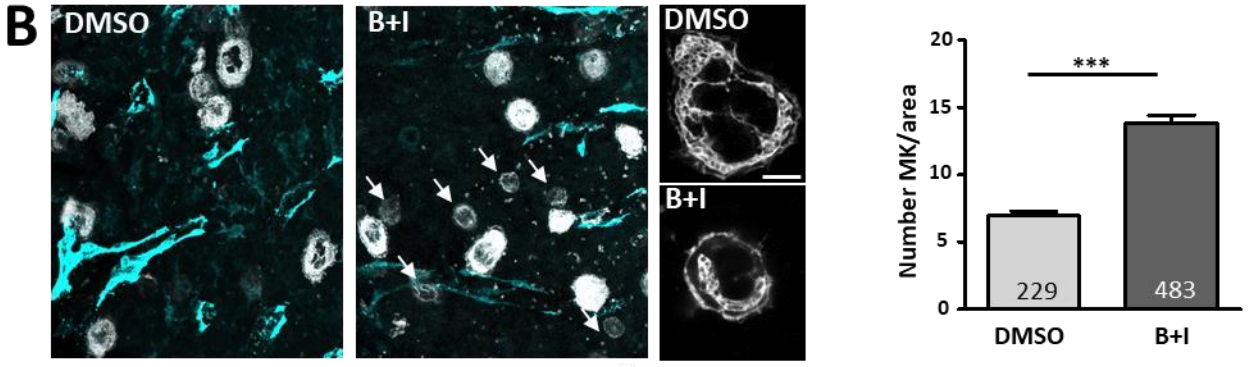
B
DMSO
B+I
Number MK/area
***
229
483

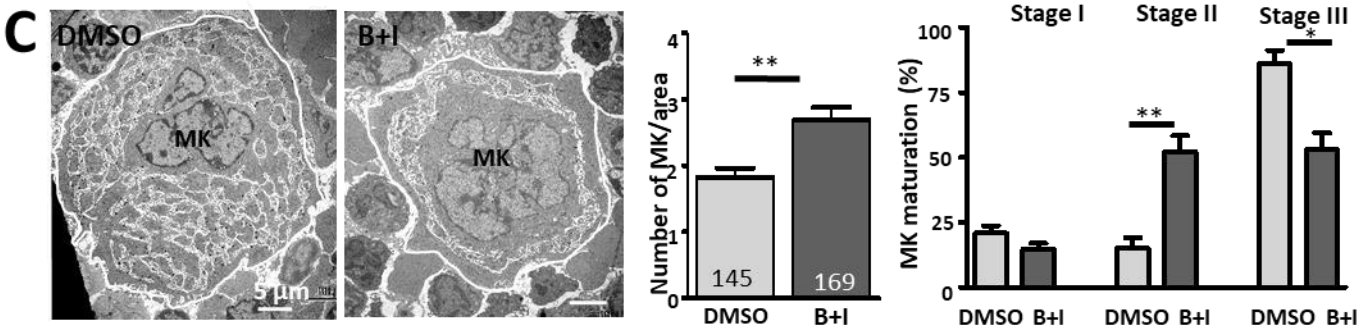
C
DMSO
B+I
MK
5 µm
Number of MK/area
**
145
169
MK maturation (%)
Stage I
Stage II
Stage III
*

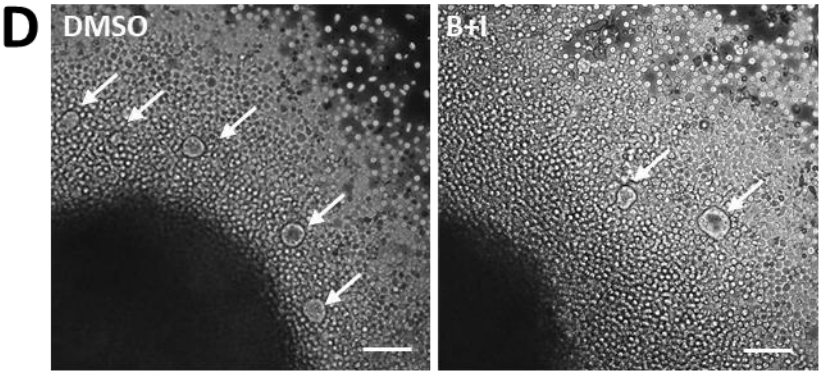
D
DMSO
B+I
Released MK
3h
6h
*

Figure 6

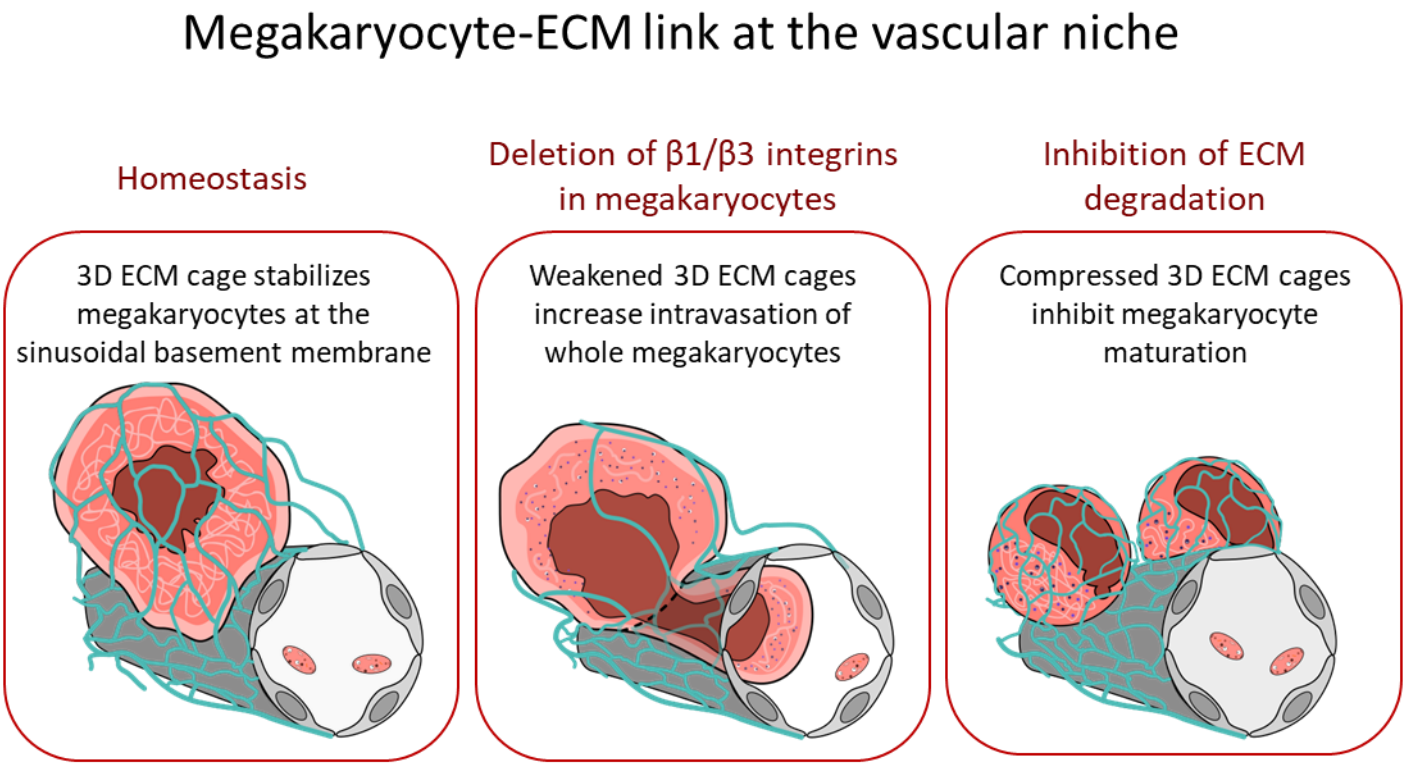
Megakaryocyte-ECM link at the vascular niche
Homeostasis
3D ECM cage stabilizes megakaryocytes at the sinusoidal basement membrane
Deletion of β1/β3 integrins in megakaryocytes
Weakened 3D ECM cages increase intravasation of whole megakaryocytes
Inhibition of ECM degradation
Compressed 3D ECM cages inhibit megakaryocyte maturation

Figure 7